



Article

## In-situ characterization of pore formation dynamics in pulsed wave laser powder bed fusion

S. Mohammad H. Hojjatzadeh <sup>1,2</sup>, Qilin Guo <sup>1,2</sup>, Niranjan D. Parab <sup>3</sup>, Minglei Qu <sup>1,2</sup>, Luis I. Escano <sup>1</sup>, Kamel Fezzaa <sup>3</sup>, Wes Everhart <sup>4</sup>, Tao Sun <sup>5, \*</sup> and Lianyi Chen <sup>2,\*</sup>

- Department of Mechanical Engineering, University of Wisconsin-Madison, Madison, Wisconsin 53706, USA.
- <sup>2</sup> Department of Materials Science and Engineering, University of Wisconsin-Madison, Madison, Wisconsin 53706, USA.
- <sup>3</sup> X-ray Science Division, Advanced Photon Source, Argonne National Laboratory, Lemont, Illinois 60439, USA.
- Department of Energy's Kansas City National Security Campus Managed by Honeywell FM&T, Kansas City, Missouri 64147, USA.
- Department of Materials Science and Engineering, University of Virginia, Charlottesville, Virginia 22904, USA.
- \* Correspondence: lianyi.chen@wisc.edu (Lianyi Chen); ts7qw@virginia.edu (Tao Sun)

**Abstract:** Laser powder bed fusion (LPBF) is an additive manufacturing technology with the capability of printing complex metal parts directly from digital models. Between two available emission modes employed in LPBF printing systems, pulsed wave (PW) emission provides more control over the heat input compared to continuous wave (CW) emission, which is highly beneficial for printing parts with intricate features. However, parts printed with pulsed wave LPBF (PW-LPBF) commonly contain pores, which degrades their mechanical properties. In this study, we reveal pore formation mechanisms during PW-LPBF in real time by using in situ high-speed synchrotron x-ray imaging technique. We found that vapor depression collapse proceeds when the laser irradiation stops within one pulse, resulting in occasional pore formation during PW-LPBF. We also revealed that the rapid melt pool solidification during pulsed-wave laser melting resulted in cavity formation and subsequent formation of pore pattern in the melted track. The pore formation dynamics revealed here may provide guidance on developing pore elimination approaches.

**Keywords:** Laser powder bed fusion; Additive manufacturing; Pore; Pulsed emission; X-ray imaging

Citation: Lastname, F.; Lastname, F.; Lastname, F. Title. *Materials* **2021**, *14*, x. https://doi.org/10.3390/xxxxx

Academic Editor: Firstname Lastname

Received: date Accepted: date Published: date

**Publisher's Note:** MDPI stays neutral with regard to jurisdictional claims in published maps and institutional affiliations.



Copyright: © 2021 by the authors. Submitted for possible open access publication under the terms and conditions of the Creative Commons Attribution (CC BY) license (https://creativecommons.org/licenses/by/4.0/).

1. Introduction

Laser powder bed fusion (LPBF) additive manufacturing (AM) process is a 3D printing technology, which selectively melts powders in successive thin layers to build three dimensional parts directly from digital models without the constraints of traditional manufacturing methods. Currently, the LPBF is rapidly growing among multiple industrial applications, such as medical, aerospace, defense, and automobile [1].

One of the primary distinctions between commercial LPBF systems, is the type of laser emission mode employed [2]. In continuous wave LPBF (CW-LPBF) systems, the laser delivers energy continuously without interruption; while in pulsed wave LPBF (PW-LPBF) systems, the laser power is fast modulated to turn on and off repeatedly, delivering energy in pulses [3,4]. The short burst of energy with PW-LPBF creates a melt pool with more flexible control over the heat input, which is highly advantageous for printing finer features such as lattice structures [5]. However, parts printed with PW-LPBF exhibit pores because the pulsated laser intrinsically causes instability in the melt pool leading to formation of pores [6]. Pore is the major defect in parts printed by LPBF AM, which adversely affects the mechanical properties [7], especially the fatigue performance [8].

46

47

48

49

50

51

52

53

54

55

56

57

58

59

60

61

62

63

64

65

66

67

68

69

70

71

72

73

74

75

76

77

78

79

80

81

82

83

84

85

While, pore formation during CW-LPBF process has been studied extensively by post-processing diagnostic techniques [9], in situ x-ray imaging technique [10–16] and high fidelity simulations [13], the research on pore formation and its underlying mechanisms during PW-LPBF is limited. Therefore, it is imperative to implement in-process diagnostic tools, such as state-of-the-art in situ x-ray imaging techniques, to perform fundamental studies on pore formation during PW-LPBF process in real time.

In this study, we revealed the dynamics and mechanisms of pore formation during the PW-LPBF process by utilizing in-situ high-speed x-ray imaging with 100 ps temporal resolution and ~2 µm spatial resolution. The results of this study are vital for developing processing parameters to mitigate pore formation and therefore improve the mechanical performance and reliability of parts printed by the PW-LPBF. In addition, the results of this research may have implications in other areas where pulsated laser is used [17–21].

## 2. Materials and Methods

High-speed high-resolution x-ray imaging (at the beamline 32-ID-B of the Advanced Photon Source, Argonne National Laboratory) was utilized to probe pore formation dynamics during PW-LPBF in real time[22]. The schematic of x-ray imaging system is displayed in Figure 1. The high-speed x-ray imaging system is composed of a miniature laser powder bed setup which is clamped between two glassy carbon as the container walls. A pseudo pink x-ray beam, with 1st harmonic energy at (24.7~25.3) keV penetrates through the metal and powder while a downstream detection system converts the transmitted x-ray beam into a visible light image using a scintillator. The converted signal is then recorded by a high-speed camera with a 10× magnification and spatial resolution of approximately 2 μm per pixel [22–25]. A recording frame rate of 50 kHz was used in this study. The experiments were performed inside a stainless-steel vacuum chamber, under 1 atm argon atmosphere. Ti-6Al-4V and Al6061 plates with the thicknesses of 0.4 and 0.7 mm, respectively, were used as the metal substrates. A layer of Al6061 powder with a thickness of ~100 µm was spread on the top of the Al6061 substrate metal to perform pulsed-LPBF AM experiments. In the experiments with Ti-6Al-4V substrate, no powder was added on the top of the substrate metal.

The key parameters to define the pulse in pulsed laser melting are frequency and laser duty cycle. The frequency (f) is defined as:

$$Frequency = \frac{1}{Period} = \frac{1}{t_{on} + t_{off}}$$
 (1)

where  $t_{\text{on}}$  is defined as the time period when the laser is "on" in each pulse, called laseron period, and  $t_{\text{off}}$  denotes the time period when laser is "off" between the end of the pulse and the beginning of the consecutive pulse, called laser-off period (see the inset of Figure 1). The laser duty cycle is the percentage of how long the laser is "on" in the given modulated period and is defined as:

$$Duty \ cycle = \frac{t_{on}}{t_{off} + t_{on}} \times 100\%$$
 (2)

An ytterbium fiber laser with the wavelength of 1070 nm, maximum output power of 520 W and a  $D4\sigma$  diameter of ~100 µm was modulated by a square wave to emit with a given peak power at varying laser frequency (up to 50 kHz) and laser duty cycle (up to 99%) to make single track laser melting on both powder bed and bare substrate samples. The laser scan velocity was varied from 0.3 to 1.5 m/s in the experiments.

The recorded x-ray images were processed using ImageJ to reduce the noise and enhance the contrast in each frame. The solid-liquid interface was identified in x-ray images by image processing where the image intensity at each pixel of Frame (i) was divided by the intensity of corresponding pixel in Frame (i+2), such that the motionless part in the image was converted to blank background [25].

Figure 1. Schematic of the x-ray imaging experiment and the temporal characteristics of PW-LPBF process. The figure shows the temporal characteristic of square shaped pulses used in the experiment and the definition of laser on and off period. Note that the actual output of the pulse shape may deviate from the perfect square shape specified in the laser control program.

3. Results

Pore formation during PW-LPBF process was studied by performing a series of x-ray imaging experiments at the frame rate of 50 kHz under varying laser frequency and laser duty cycle. Figure 2 and Supplementary Movies 1-3 show pore formation during PW-LPBF process of Al6061 under varying laser frequency (4, 7, and 10 kHz) and a constant laser duty cycle (50%). Pores are observed to form occasionally via the rapid collapse of the vapor depression at the end of the laser-on period in one pulse which is reminiscence of pore formation at the end of laser track during CW-LPBF AM. The mechanism of pore formation when the laser is turned off at the end of the track has been extensively studied before[11,13,15,22]. Under constant laser duty cycle (while laser power and scan speed are also kept constant), the melt pool size is observed to be the function of laser frequency. As the laser frequency increased (from 4 to 10 kHz), smaller melt pool and therefore shallower depression zone formed. This caused formation of pores from vapor depression collapse at the depth closer to the interface between the substrate and the powder layer, as can be directly observed in Figure 2.

90 91

86

87

88

89

92

93

94 95 96

110111

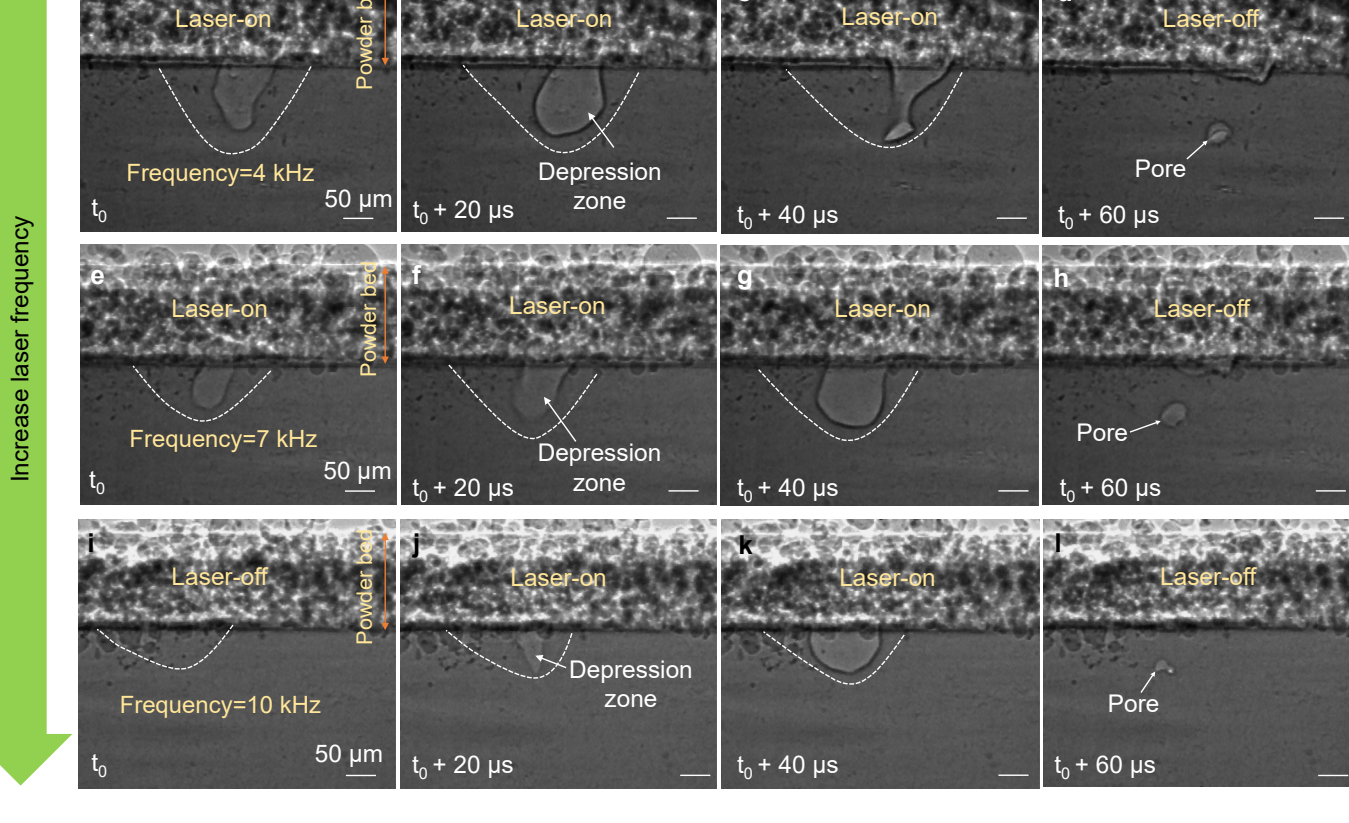


**Figure 2.** Pore formation under varying laser frequencies at a constant laser duty cycle: (**a-1**) Dynamic x-ray images showing pore formation during PW-LPBF of Al6061 at laser frequencies of 4 kHz (**a-d**); 7 kHz (**e-h**); and 10 kHz (**i-l**) under a laser duty cycle of 50%, a laser power of 470 W and a scan speed of 0.4 m/s. In d, h and l, the melt pool boundary is not indicated to avoid blocking the pores. Note that images do not display the complete duration of one pulse. The compiled movies showing complete duration of two consecutive pulses are available in the Supplementary Material.

Similarly, vapor depression collapse at the end of laser on period occasionally caused pore formation in the melt pool under varying laser duty cycle and a constant laser frequency, as shown in Figure 3 and Supplementary Movies 4-6. The increase in laser duty cycle and therefore longer laser exposure time in these experiments resulted in formation of larger melt pool and subsequently formation of pore at the larger depth relative to the interface between the substrate and the powder layer. From these experimental observations, neither the size nor the number of pores were identified to be correlated with the change of laser frequency or duty cycle (Figures 2 and 3), which is ascribed to the random pore formation from vapor depression collapse during PW-LPBF.

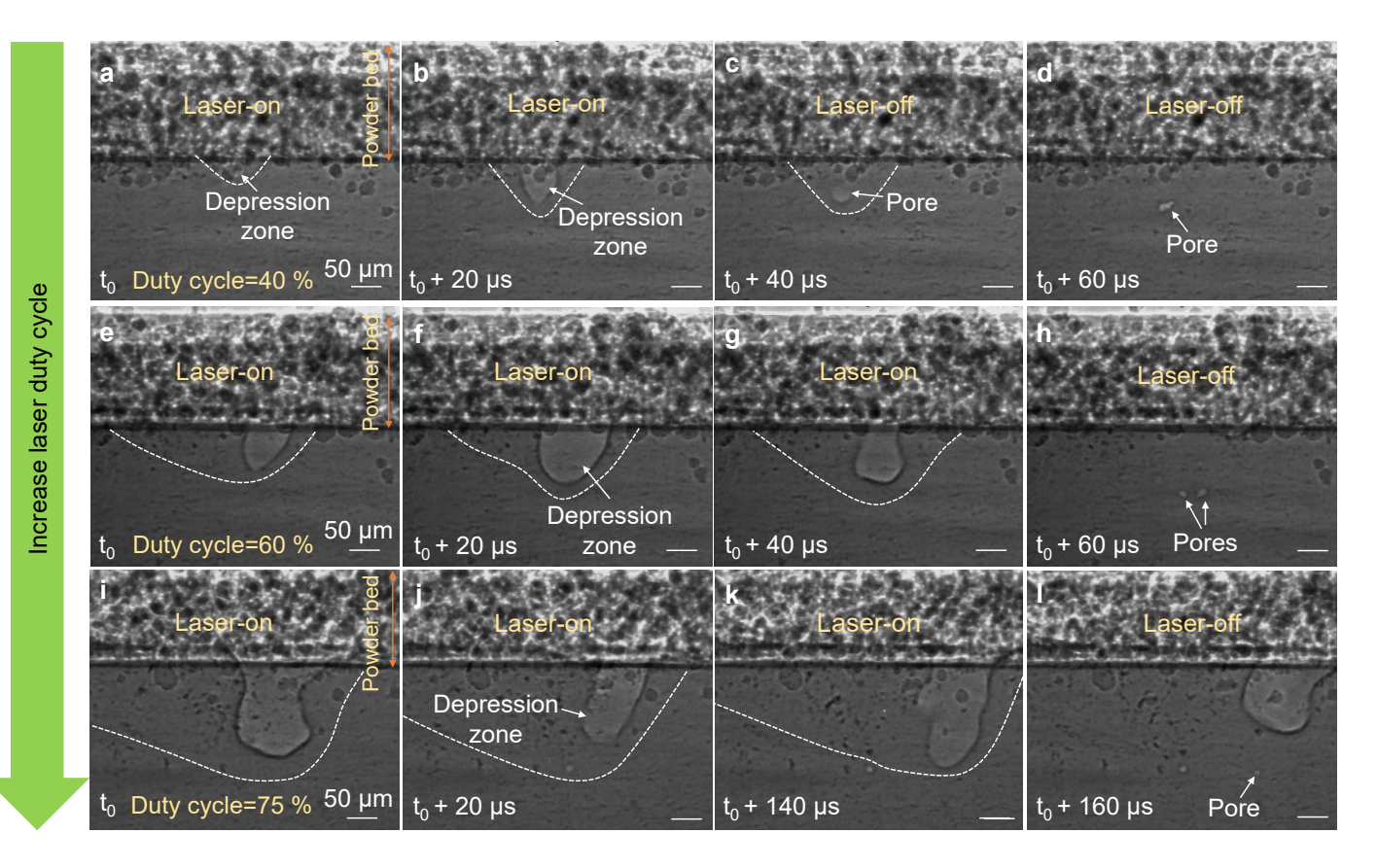


**Figure 3.** Pore formation under varying laser duty cycles at a constant laser frequency: (a-l) Dynamic x-ray images showing pore formation during PW-LPBF process of Al6061 at the laser duty cycle of 40% (a-d); 60% (e-h); and 75% (i-l) at a laser frequency of 7 kHz, a laser power of 470 W and a scan speed of 0.4 m/s. In d, h and l, the melt pool boundary is not indicated to avoid blocking the pores view. Note images do not display the complete duration of one pulse. The compiled movies showing the complete duration of two consecutive pulses are available in the Supplementary Material.

Low laser frequency is associated with longer pulse duration ( $period = \frac{1}{frequency}$ ) and therefore longer laser irradiation time. To further our understanding of pore formation at low laser frequency, we performed a series of x-ray imaging experiments during pulsed-wave laser melting of Ti-6Al-4V at 4 kHz under varying laser duty cycle. Figure 4 and Supplementary Movie 7 display the x-ray image sequences during pulsed-wave laser melting of Ti-6Al-4V substrate at a laser frequency of 4 kHz and a duty cycle of 50%. The first frame (to, Figure 4a) shows the onset of the laser pulse when laser irradiation starts. Within 120 µs, the laser irradiation stops, leading to a rapid freezing of the melt pool and formation of a cavity, mirroring the shape of the depression zone (Figure 4d). As the consecutive laser pulse begins, the depression zone emerges at a location of ~220 µm far away from the center of the first cavity (to + 300 µs, Figure 4f). The laser irradiation stops again after 120 µs and resulted in formation of the second cavity in the substrate (Figure 4h). As the laser moves forward, the cavity formation proceeds and a pattern of cavity is formed in the substrate material (to + 900 µs, Figure 4p).

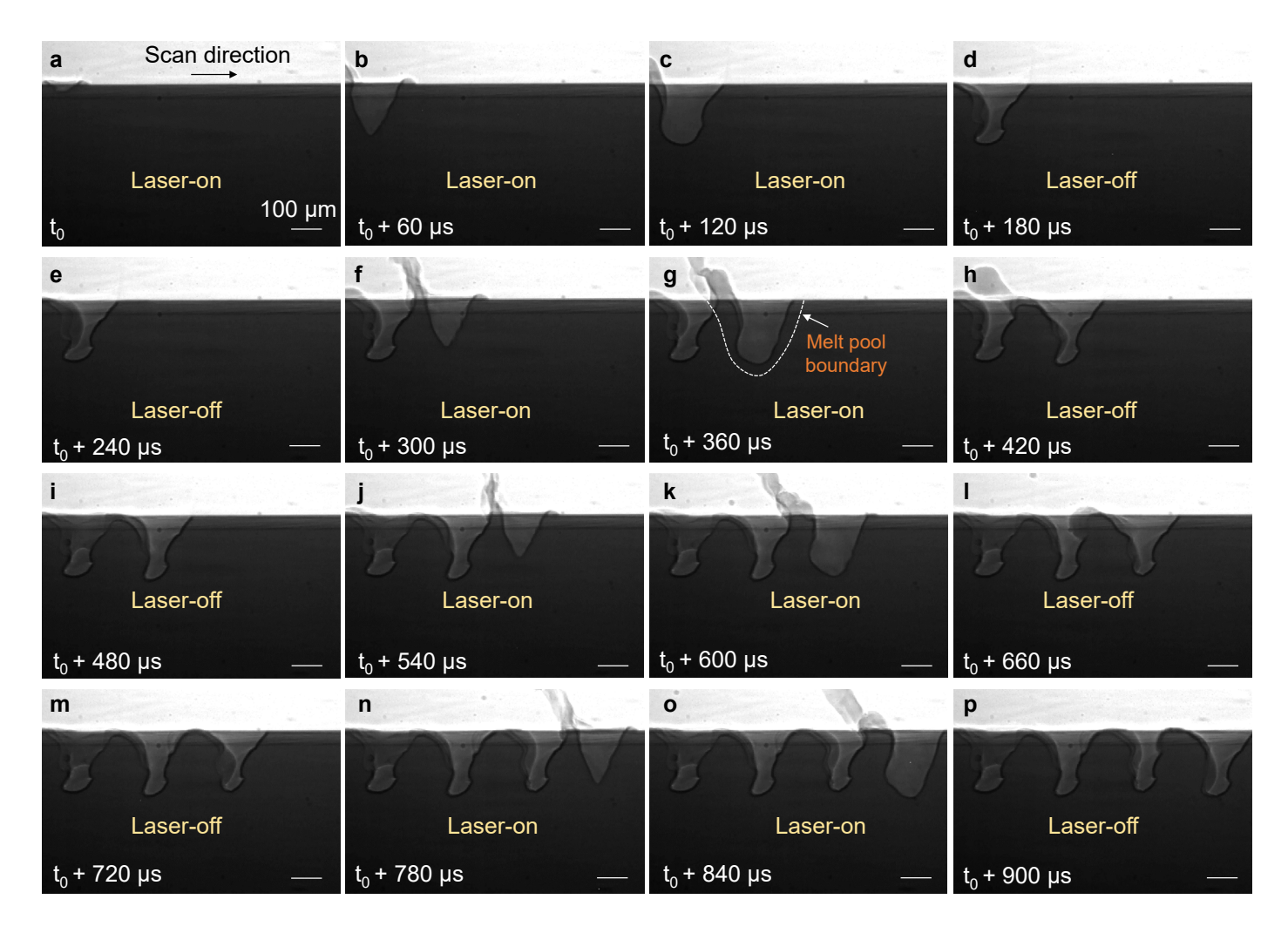


**Figure 4.** Cavity pattern formation at low laser frequency: (a-p) Dynamic x-ray images showing formation of cavity during pulsed-wave laser melting of Ti-6Al-4V substrate at a laser frequency of 4 kHz, a duty cycle of 50%, a laser power of 420 W, and a scan speed of 0.8 m/s. Note that some image frames during laser-on time and laser-off time have been skipped. The compiled movies showing the details are available in the Supplementary Material.

In the modulated laser, the distance that laser travels at the time interval between pulses (commonly called as the point distance) is decreased via the decrease in laser scan speed. This results in formation of the overlap between melt pools of the consecutive pulses. Figure 5 and Supplementary Movie 8 show x-ray imaging experiment during pulsed-wave laser melting of Ti-6Al-4V substrate at a laser frequency of 4 kHz, a duty cycle of 60% and a laser scan speed of 0.5 m/s. The cavity forms after the rapid freezing of the melt pool at the end of laser on period. As the consecutive pulse begins, the vapor depression emerges at a location where it interacts with the cavity, turning the cavity into a closed pore (Figure 5 a-o). As the laser melting continues, a pattern of pore forms in the substate via this pore formation mechanism (Figure 5p).



**Figure 5.** Pore pattern formation from cavity at low laser frequency: (a-p) Dynamic x-ray images showing the formation of pore from the cavity during pulsed-wave laser melting of Ti-6Al-4V at a laser frequency of 4 kHz, a duty cycle of 60%, a laser power of 470 W and a laser scan speed of 0.5 m/s. The pore formation from cavity in two consecutive pulses has been shown in (a-o). Note that some image frames during laser-on period and laser-off period have been skipped. The movies showing pore formation dynamics are available in the Supplementary Material.

4. Discussion

We constructed schematics to illustrate the formation mechanisms of the cavity pattern and pore pattern. The mechanism of cavity pattern formation is displayed in Figure 6a-f. During the laser melting, vapor cavity is formed progressively in the substrate material by a strong vaporization induced recoil pressure. The melt pool that forms in one pulse is observed to be only slightly larger than the vapor depression (as indicated in Figure 4g), appearing to form a layer of liquid around the vapor depression. A strong recoil pressure around the vapor depression pushes the molten metal to move rapidly along the vapor depression walls and ultimately ejects away near the rim of the vapor depression in the form of a melt ligament and spatter (Figures 6b and c). As a result, a large amount of liquid metal is ejected away rapidly from the melted area around the vapor depression during laser melting. This phenomenon was recently simulated by a high-fidelity model [13]. As the laser turns off, the temperature at the back of the depression zone decreases abruptly, which results in rapid solidification of the remaining liquid around the vapor depression, before the liquid fills the cavity (Figures 4h and 6d-f).

186

187

188

189

190

191

192

193

194

195

196

197

198

199

200

201

202

203

204

At the laser parameters setting used here, we did not observe the cavity pattering mechanism in Al6061 substrates. This can be ascribed to the higher thermal conductivity of Al6061 relative to Ti-6Al-4V (90 W/mK compared to 35 W/mK [26,27]). In Ti-6Al-4V, pulsed laser melting results in formation of a small melt pool in each pulse which starts to cool and solidify as soon as the pulse is complete. In Al6061 substrate material with higher thermal conductivity, on the other hand, a larger melt pool with longer solidification time forms in each pulse, which appears like a continuous melt pool by looking at consecutive pulses. As the laser irradiation stops in each pulse, there is sufficient melt around the vapor depression to reverse the direction towards the vapor depression side walls and fills the vapor cavity [28]. Similar cavity formation phenomena may be observed in Al6061 substrate by reducing the pulse duration and increasing the laser power. The mechanism of pore pattern formation from cavity is schematically shown in Figure 6g-l. The first cavity forms as a result of rapid solidification of the melt pool when laser is switched off at the end of the laser-on period (Figure 6g-i). With the onset of the consecutive pulse, a new melt pool is created where it connects with the cavity formed in the previous pulse (Figure 6j). As the melted zone moves forward and grows in depth with the laser translating, the upper and middle portion of the cavity is filled with the liquid flowing from the melt pool, and the bottom portion of the cavity remains as a closed pore in the substrate material (Figure 6j-l). This process can continue until a pattern of pore is observed in the substrate material.

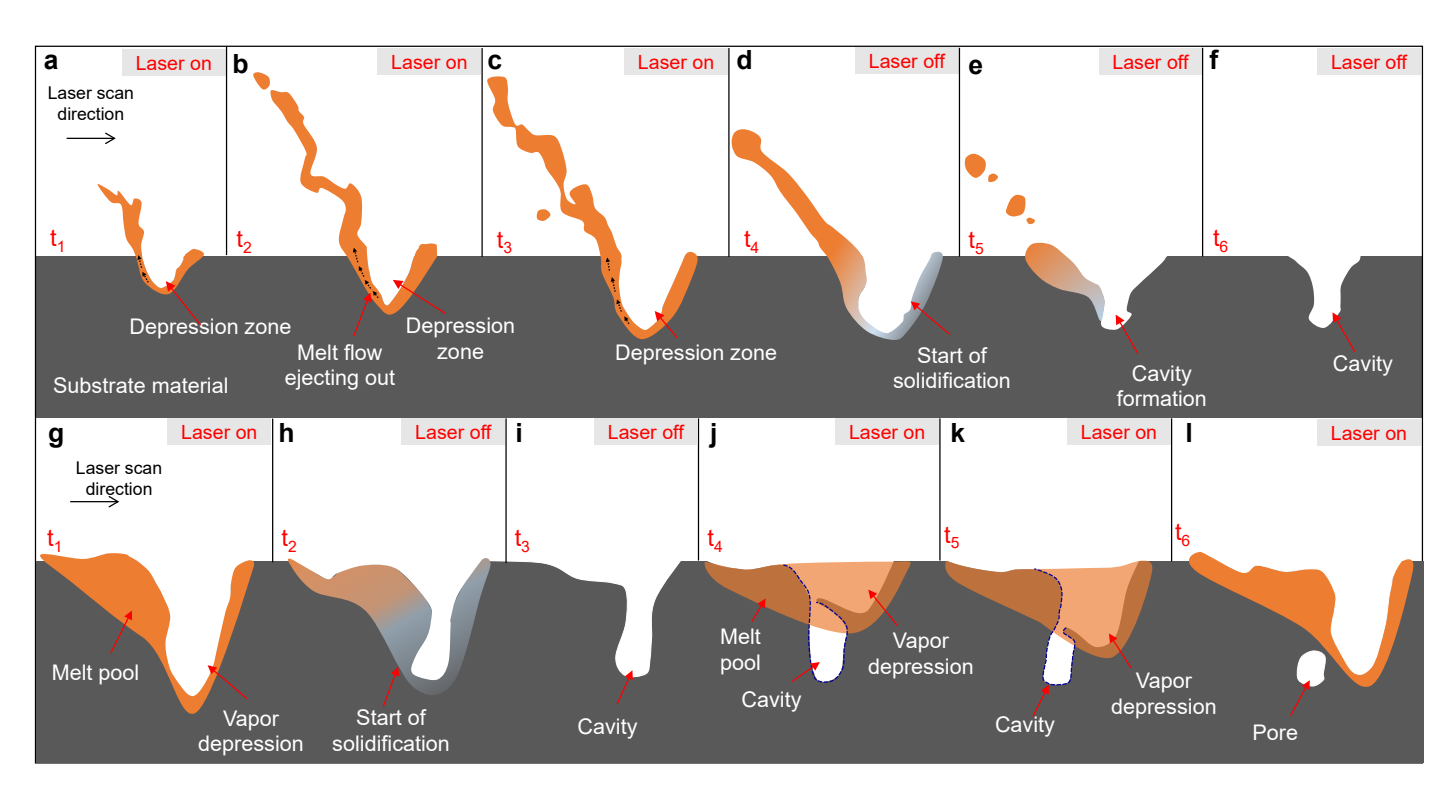


**Figure 6.** The mechanisms of pore and cavity pattern formation at low laser frequency: (**a-f**) Cavity formation mechanism; (**g-l**) Mechanism of pore formation from cavity at low laser frequency.

5. Conclusions

In summary, pore formation dynamics during pulsed wave LPBF AM process was directly observed by utilizing synchrotron x-ray imaging technique. The main conclusions are as follows:

205

207

208

209

210

- 1. The collapse of vapor depression, when laser irradiation stops at the end of laser on period in one pulse, was observed to occasionally induce pores during PW-LPBF process under varying laser frequencies and duty cycles.
- 2. The melt pool and depression zone size changed with laser frequency and duty cycle. With increase of the laser frequency or decrease of the duty cycle, the melt pool size and consequently depression zone size decreased during PW-LPBF.
- 3. Our experimental observations did not reveal any correlation between the size nor the number of pores and the laser frequency or duty cycle.
- 5. In the depression/keyhole mode laser melting, at a low laser frequency with large point distance, cavity formation proceeds via the rapid solidification of the thin molten metal layer around the vapor cavity, which subsequently results in the formation of cavity pattern in the substrate material.
- 6. In the depression/keyhole mode laser melting, at a low laser frequency with small point distance, the interaction of the cavity with the melt pool in the consecutive pulse results in the formation of closed pores and pore pattern.
- 7. The results of this study will help the understanding of the PW-LPBF process and guide the development of processing approaches to mitigate pores.

**Supplementary Materials:** The following are available online at www.mdpi.com/xxx/s1, Movie S1: The dynamics of pore formation during pulsed wave LPBF of Al6061 at a laser frequency of 4 kHz, duty cycle of 50%, laser power of 470 W, and laser scan speed of 0.4 m/s; Movie S2: The dynamics of pore formation during pulsed wave LPBF of Al6061 at a laser frequency of 7 kHz, duty cycle of 50%, laser power of 470 W, and laser scan speed of 0.4 m/s; Movie S3: The dynamics of pore formation during pulsed wave LPBF of Al6061 at a laser frequency of 10 kHz, duty cycle of 50%, laser power of 470 W, and laser scan speed of 0.4 m/s; Movie S4: The dynamics of pore formation during pulsed wave LPBF of Al6061 at a duty cycle of 40%, laser frequency of 7 kHz, laser power of 470 W, and laser scan speed of 0.4 m/s; Movie S5: The dynamics of pore formation during pulsed wave LPBF of Al6061 at a duty cycle of 60%, laser frequency of 7 kHz, laser power of 470 W, and laser scan speed of 0.4 m/s; Movie S6: The dynamics of pore formation during pulsed wave LPBF of Al6061 at a duty cycle of 75%, laser frequency of 7 kHz, laser power of 470 W, and laser scan speed of 0.4 m/s; Movie S7: The dynamics of cavity pattern formation during pulsed-wave laser melting of Ti-6Al-4V substrate at a laser frequency of 4 kHz, duty cycle of 50%, laser power of 420 W, and scan speed of 0.8 m/s; Movie S8: The dynamics of pore pattern formation during pulsed-wave laser melting of Ti-6Al-4V substrate at a laser frequency of 4 kHz, duty cycle of 60%, laser power of 470 W and laser scan speed of 0.5 m/s.

**Author Contributions:** L.C.: Conceptualization, Supervision. T.S., N.D.P, L.C., S.M.H.H., and W.E. Methodology. Q.G., T.S., N.D.P., S.M.H.H., L.I.E., M.Q., K.F., W.E., L.C.: Investigation. S.M.H.H. and L.C.: Formal analysis. All authors discussed the results. S.M.H.H. and L.C. Writing - Original draft with input from all authors, Writing - Review & Editing.

Acknowledgments: The authors would like to thank Alex Deriy at Advanced Photon Source for his help on the beamline experiments. This research used resources of the Advanced Photon Source, a U.S. Department of Energy (DOE) Office of Science User Facility operated for the DOE Office of Science by Argonne National Laboratory under Contract No. DE-AC02-06CH11357. This work is funded by the Department of Energy's Kansas City National Security Campus Managed by Honeywell Federal Manufacturing & Technologies (FM&T) and National Science Foundation. All data prepared, analyzed and presented have been developed in a specific context of work and was prepared for internal evaluation and use pursuant to that work authorized under the referenced contract. Reference herein to any specific commercial product, process or service by trade name, trademark, manufacturer, or otherwise, does not necessarily constitute or imply its endorsement, recommendation, or favoring by the United States Government, any agency thereof or Honeywell Federal Manufacturing & Technologies, LLC. This publication has been authored by Honeywell Federal Manufacturing & Technologies under Contract No. DE-NA0002839 with the U.S. Department of

271

272

273

274

275

276

277

278

279

280

286

287

288

291

292

293

294

295

296

Energy. The United States Government retains and the publisher, by accepting the article for publi-
cation, acknowledges that the United States Government retains a nonexclusive, paid up, irrevoca-
ble, world-wide license to publish or reproduce the published form of this manuscript, or allow
others to do so, for the United States Government purposes.
Conflicts of Interest: The authors declare no conflict of interest.

References

- 270
- 1. Herzog, D.; Seyda, V.; Wycisk, E.; Emmelmann, C. Additive manufacturing of metals. Acta Mater. 2016, 117, 371-392, doi:10.1016/j.actamat.2016.07.019.
- Kim, J.; Ji, S.; Yun, Y.; Yeo, J. A review: melt pool analysis for selective laser melting with continuous wave and 2. pulse width modulated lasers. Appl. Sci. Converg. Technol. 2018, 27, 113–119, doi:10.5757/ASCT.2018.27.6.113.
- 3. Demir, A.G.; Colombo, P.; Previtali, B. From pulsed to continuous wave emission in SLM with contemporary fiber laser sources: effect of temporal and spatial pulse overlap in part quality. Int. J. Adv. Manuf. Technol. 2017, 91, 2701-2714, doi:10.1007/s00170-016-9948-7.
- 4. Saunders, M. Modulation matters - how to build all features great and small. 2018, 1-7, doi:https://resources.renishaw.com/en/details/feature-article-modulation-matters-how-to-build-all-featuresgreat-and-small--113986.
- 5. Demir, A.G.; Previtali, B. Additive manufacturing of cardiovascular CoCr stents by selective laser melting. *Mater*. 281 Des. 2017, 119, 338–350, doi:10.1016/j.matdes.2017.01.091. 282
- 6. Kuo, T.Y.; Lin, Y.D. Effects of different shielding gases and power waveforms on penetration characteristics and porosity formation in laser welding of inconel 690 alloy. Mater. Trans. 2007, 48, 219-226, doi:10.2320/matertrans.48.219. 285
- 7. DebRoy, T.; Wei, H.L.; Zuback, J.S.; Mukherjee, T.; Elmer, J.W.; Milewski, J.O.; Beese, A.M.; Wilson-Heid, A.; De, A.; Zhang, W. Additive manufacturing of metallic components – process, structure and properties. Prog. Mater. Sci. 2018, 92, 112–224, doi:10.1016/j.pmatsci.2017.10.001.
- Kasperovich, G.; Hausmann, J. Improvement of fatigue resistance and ductility of TiAl6V4 processed by selective 8. 289 laser melting. J. Mater. Process. Technol. 2015, 220, 202–214, doi:10.1016/j.jmatprotec.2015.01.025. 290
- 9. Cunningham, R.; Nicolas, A.; Madsen, J.; Fodran, E.; Anagnostou, E.; Sangid, M.D.; Rollett, A.D. Analyzing the effects of powder and post-processing on porosity and properties of electron beam melted Ti-6Al-4V. Mater. Res. Lett. 2017, 5, 516–525, doi:10.1080/21663831.2017.1340911.
- 10. Leung, C.L.A.; Marussi, S.; Atwood, R.C.; Towrie, M.; Withers, P.J.; Lee, P.D. In situ X-ray imaging of defect and molten pool dynamics in laser additive manufacturing. Nat. Commun. 2018, 9, 1355, doi:10.1038/s41467-018-03734-7.
- Martin, A.A.; Calta, N.P.; Hammons, J.A.; Khairallah, S.A.; Nielsen, M.H.; Shuttlesworth, R.M.; Sinclair, N.; 11. 297 Matthews, M.J.; Jeffries, J.R.; Willey, T.M.; et al. Ultrafast dynamics of laser-metal interactions in additive 298 manufacturing alloys captured by in situ X-ray imaging. Mater. Today Adv. 2019, 1, 100002, 299

doi:10.1016/j.mtadv.2019.01.001.

- 300
- 12. Gould, B.; Wolff, S.; Parab, N.; Zhao, C.; Lorenzo-Martin, M.C.; Fezzaa, K.; Greco, A.; Sun, T. In situ analysis of 301 laser powder bed fusion using simultaneous high-speed infrared and x-ray imaging. JOM 2021, 73, 201-211, doi:10.1007/s11837-020-04291-5. 303

13. Khairallah, S.A.; Martin, A.A.; Lee, J.R.I.; Guss, G.; Calta, N.P.; Hammons, J.A.; Nielsen, M.H.; Chaput, K.; Schwalbach, E.; Shah, M.N.; et al. Controlling interdependent meso-nanosecond dynamics and defect generation in metal 3D printing. Science. 2020, 368, 660-665, doi:10.1126/science.aay7830.

304 305

306

14. Hojjatzadeh, S.M.H.; Parab, N.D.; Guo, Q.; Qu, M.; Xiong, L.; Zhao, C.; Escano, L.I.; Fezzaa, K.; Everhart, W.; Sun, T.; et al. Direct observation of pore formation mechanisms during LPBF additive manufacturing process and energy density laser welding. Int. I. Mach. Tools Manuf. doi:10.1016/j.ijmachtools.2020.103555.

308 309

307

15. Martin, A.A.; Calta, N.P.; Khairallah, S.A.; Wang, J.; Depond, P.J.; Fong, A.Y.; Thampy, V.; Guss, G.M.; Kiss, A.M.; Stone, K.H.; et al. Dynamics of pore formation during laser powder bed fusion additive manufacturing. Nat. Commun. 2019, 10, 1-10, doi:10.1038/s41467-019-10009-2.

310 311

312

313

16. Cunningham, R.; Zhao, C.; Parab, N.; Kantzos, C.; Pauza, J.; Fezzaa, K.; Sun, T.; Rollett, A.D. Keyhole threshold and morphology in laser melting revealed by ultrahigh-speed x-ray imaging. Science. 2019, 363, 849-852, doi:10.1126/science.aav4687.

314 315

17. Gao, X.-L.; Zhang, L.-J.; Liu, J.; Zhang, J.-X. Porosity and microstructure in pulsed Nd:YAG laser welded Ti6Al4V sheet. J. Mater. Process. Technol. 2014, 214, 1316–1325, doi:10.1016/j.jmatprotec.2014.01.015.

316 317

318

18. AlShaer, A.W.; Li, L.; Mistry, A. The effects of short pulse laser surface cleaning on porosity formation and reduction in laser welding of aluminium alloy for automotive component manufacture. Opt. Laser Technol. 2014, 64, 162–171, doi:10.1016/j.optlastec.2014.05.010.

319 320

321

19. Perry, T.L.; Werschmoeller, D.; Li, X.; Pfefferkorn, F.E.; Duffie, N.A. Pulsed laser polishing of micro-milled Ti6Al4V samples. J. Manuf. Process. 2009, 11, 74–81, doi:10.1016/j.jmapro.2009.10.001. 323

322

20. Wu, Z.; Yin, K.; Wu, J.; Zhu, Z.; Duan, J.-A.; He, J. Recent advances in femtosecond laser-structured Janus 324 membranes with asymmetric surface wettability. Nanoscale 2021, 13, 2209–2226, doi:10.1039/D0NR06639G. 325

21. Gao, X.; Feng, W.; Zhu, Z.; Wu, Z.; Li, S.; Kan, S.; Qiu, X.; Guo, A.; Chen, W.; Yin, K. Rapid Fabrication of Superhydrophilic Micro/Nanostructured Nickel Foam Toward High-Performance Glucose Sensor. Adv. Mater. Interfaces 2021, 8, 2002133, doi:10.1002/admi.202002133.

326 327

22. Hojjatzadeh, S.M.H.; Parab, N.D.; Yan, W.; Guo, Q.; Xiong, L.; Zhao, C.; Qu, M.; Escano, L.I.; Xiao, X.; Fezzaa, K.; et al. Pore elimination mechanisms during 3D printing of metals. Nat. Commun. 2019, 10, 3088, doi:10.1038/s41467-019-10973-9.

328 329

23. Zhao, C.; Fezzaa, K.; Cunningham, R.W.; Wen, H.; De Carlo, F.; Chen, L.; Rollett, A.D.; Sun, T. Real-time

331 332

monitoring of laser powder bed fusion process using high-speed X-ray imaging and diffraction. Sci. Rep. 201	7,
7, 3602, doi:10.1038/s41598-017-03761-2.	

- 24. Guo, Q.; Zhao, C.; Escano, L.I.; Young, Z.; Xiong, L.; Fezzaa, K.; Everhart, W.; Brown, B.; Sun, T.; Chen, L. Transient dynamics of powder spattering in laser powder bed fusion additive manufacturing process revealed by in-situ high-speed high-energy x-ray imaging. *Acta Mater.* **2018**, *151*, 169–180, doi:10.1016/j.actamat.2018.03.036.
- 25. Guo, Q.; Zhao, C.; Qu, M.; Xiong, L.; Escano, L.I.; Hojjatzadeh, S.M.H.; Parab, N.D.; Fezzaa, K.; Everhart, W.; Sun, T.; et al. In-situ characterization and quantification of melt pool variation under constant input energy density in laser powder bed fusion additive manufacturing process. *Addit. Manuf.* **2019**, 28, 600–609, doi:10.1016/j.addma.2019.04.021.
- 26. Ning, J.; Mirkoohi, E.; Dong, Y.; Sievers, D.E.; Garmestani, H.; Liang, S.Y. Analytical modeling of 3D temperature distribution in selective laser melting of Ti-6Al-4V considering part boundary conditions. *J. Manuf. Process.* **2019**, 44, 319–326, doi:10.1016/j.jmapro.2019.06.013.
- 27. Jagadeesh, S.K.; Ramesh, C.S.; Mallikarjuna, J.M.; Keshavamurthy, R. Prediction of cooling curves during solidification of Al 6061-SiCp based metal matrix composites using finite element analysis. *J. Mater. Process. Technol.* **2010**, 210, 618–623, doi:10.1016/j.jmatprotec.2009.11.010.
- 28. Khairallah, S.A.; Anderson, A.T.; Rubenchik, A.; King, W.E. Laser powder-bed fusion additive manufacturing: physics of complex melt flow and formation mechanisms of pores, spatter, and denudation zones. *Acta Mater*. **2016**, *108*, 36–45, doi:10.1016/j.actamat.2016.02.014.